Two Lipid-Packing Sensor Motifs Contribute to the Sensitivity of ArfGAP1 to Membrane Curvature †

7 AUTHORS, INCLUDING:

Bruno Mesmin
University of Nice-Sophia Antipolis
17 PUBLICATIONS 709 CITATIONS

SEE PROFILE

Sharon Tal
University of Haifa
8 PUBLICATIONS 169 CITATIONS

SEE PROFILE

Dan Cassel
Technion - Israel Institute of Technology
49 PUBLICATIONS 2,566 CITATIONS

SEE PROFILE

Joelle Bigay
University of Nice-Sophia Antipolis
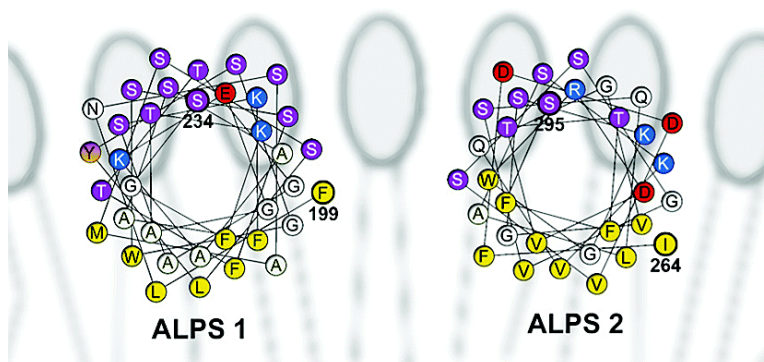33 PUBLICATIONS 2,227 CITATIONS

SEE PROFILE

Article

Two Lipid-Packing Sensor Motifs Contribute to
the Sensitivity of ArfGAP1 to Membrane Curvature

Bruno Mesmin, Guillaume Drin, Sharon Levi, Moran Rawet, Dan Cassel, Jolle Bigay, and Bruno Antonny

More About This Article

Additional resources and features associated with this article are available within the HTML version:

- Supporting Information
- Links to the 5 articles that cite this article, as of the time of this article download
- Access to high resolution figures
- Links to articles and content related to this article
- Copyright permission to reproduce figures and/or text from this article

View the Full Text HTML

Two Lipid-Packing Sensor Motifs Contribute to the Sensitivity of ArfGAP1 to Membrane Curvature[†]

Bruno Mesmin,[‡] Guillaume Drin,[‡] Sharon Levi,[§] Moran Rawet,[§] Dan Cassel,[§] Joëlle Bigay,[‡] and Bruno Antonny*,[‡]

Institut de Pharmacologie Moléculaire et Cellulaire, CNRS et Université de Nice-Sophia Antipolis, 06560 Valbonne, France, and Department of Biology, Technion-Israel Institute of Technology, Haifa 32000, Israel

ABSTRACT: ArfGAP1 (Arf GTPase activating protein 1) controls the cycling of the COPI coat on Golgi membranes by catalyzing GTP hydrolysis in the small G protein Arf1. ArfGAP1 contains a central motif named ALPS (ArfGAP1 lipid-packing sensor) that adsorbs preferentially onto highly curved membranes. This motif allows coupling of the rate of GTP hydrolysis in Arf1 with membrane curvature induced by the COPI coat. Upon membrane adsorption, the ALPS motif folds into an amphipathic α-helix. This helix contrasts from a classical membrane-adsorbing helix in the abundance of S and T residues and the paucity of charged residues in its polar face. We show here that ArfGAP1 contains a second motif with similar physicochemical properties. This motif, ALPS2, also forms an amphipathic α-helix at the surface of small vesicles and contributes to the Golgi localization of ArfGAP1 in vivo. Using several quantitative assays, we determined the relative contribution of the two ALPS motifs in the recognition of liposomes of defined curvature and composition. Our results show that ALPS1 is the primary determinant of the interaction of ArfGAP1 with lipid membranes and that ALPS2 reinforces this interaction 40-fold. Furthermore, our results suggest that depending on the engagement of one or two functional ALPS motifs, ArfGAP1 can respond to a wide range of membrane curvature and can adapt to lipid membranes of various acyl chain compositions.

The COPI coat drives the budding of small transport vesicles from the Golgi apparatus (*1*, *2*). Like other protein coats, it shapes mechanically the lipid membrane into a spherical structure (diameter of ca. 60 nm) and selects cargo proteins for transport. COPI assembly begins with the translocation of the small G protein Arf1 upon GDP−GTP exchange, a reaction that is catalyzed by specific guanine nucleotide exchange factors associated with Golgi membranes. Membrane-bound Arf1-GTP then recruits coatomer, a large cytosolic complex that is somewhat similar with clathrin and its adaptors (*3*). After being recruited, coatomer polymerizes into a coat and interacts with the cytosolic extension of membrane proteins, thereby facilitating their incorporation into the nascent vesicle. In analogy with other protein coats, membrane deformation probably results from the intrinsic curvature of the COPI lattice as well as the partial embedding of the N-terminal myristoylated amphipathic helix of Arf1-GTP in the lipid bilayer (*4*).

GTP hydrolysis in Arf1 is required for the disassembly of the COPI coat. This reaction, which is catalyzed in the Golgi by specific GTPase activating proteins (ArfGAP1[1] and ArfGAP3 in mammals and Gcs1p and Glo3p in yeast), must be finely tuned and somehow linked to the completion of vesicle formation in terms of both cargo recruitment and membrane shaping (*5*). Thus, if the concentration of cargo molecules is too low in a COPI-coated area, GTP hydrolysis may serve to promote early coat disassembly before the formation of a useless "empty" vesicle. On the other hand, if there are enough cargo molecules incorporated, GTP hydrolysis should be tuned to permit coat disassembly only after vesicle formation. At the molecular level, several mechanisms for the control of GTP hydrolysis in Arf1 have been envisaged, which are based on the multiple interactions that ArfGAPs can make in a COPI-coated area: with coatomer (*6−8*), with the cytoplasmic region of membrane proteins (*8−10*), and with the lipid membrane (*11−13*).

ArfGAP1 is a 415-amino acid cytosolic protein that associates in a dynamic manner with the Golgi apparatus where it controls COPI coat cycling (*14*, *15*). The first 136 residues of ArfGAP1 form the GAP catalytic domain, which is built on a characteristic Zn-finger fold and promotes GTP hydrolysis on Arf1. After the GAP domain and up to the C-terminus, no other well-defined structural domain has been identified. Instead, limited-proteolysis experiments and cir-

[1] Abbreviations: ALPS, ArfGAP1 lipid-packing sensor; ArfGAP1, Arf GTPase activating protein 1; CD, circular dichroism; DLS, dynamic light scattering; DOPE, 1,2-dioleoyl-*sn*-glycero-3-phosphoethanolamine; DOPC, 1,2-dioleoyl-*sn*-glycero-3-phosphocholine; GST, glutathione *S*-transferase; MRE, mean residue ellipticity; NBD, 7-nitrobenz-2-oxa-1,3-diazole.

cular dichroism (CD) measurements suggest that the non-catalytic region of ArfGAP1 may be largely unfolded (*6*, *16*). It is in this poorly defined region where the information for the targeting of ArfGAP1 to the Golgi apparatus resides (*15*, *17*, *18*). The molecular detail of this targeting is not known, but a combination of interactions with transmembrane proteins, with the COPI coat, and with lipids is likely.

In vitro, the activity of ArfGAP1 is highly sensitive to membrane curvature. Using model liposomes of a defined size, we showed that the rate of GTP hydrolysis in membrane-bound Arf1 catalyzed by ArfGAP1 increases by up to 2 orders of magnitude as the liposome radius decreases from ca. 150 to 30 nm, a range of curvature that is typical of coat-driven budding reactions (*19*). Because the effect of membrane curvature on ArfGAP1 activity also applies when Arf1-GTP is engaged in the COPI coat, we suggested a negative feedback loop where COPI assembly drives membrane curvature, which in turn prepares the coat for disassembly by recruiting and/or activating ArfGAP1, thereby promoting GTP hydrolysis in Arf1 (*19*). We have recently identified a motif within the noncatalytic region of ArfGAP1 that responds to membrane curvature (*16*). This motif of ∼40 residues named ALPS (for ArfGAP1 lipid-packing sensor) is located at the center of the primary sequence, around W211. In solution, the ALPS motif is not structured. However, at the surface of highly curved membranes, it forms an amphipathic α-helix. The most noticeable feature of this α-helix is the abundance of serine and threonine residues in its polar face (*4*, *16*). Because Ser and Thr cannot make electrostatic interactions with lipid polar heads, the adsorption and/or folding of the ALPS motif is driven solely by the insertion of hydrophobic residues between lipids and is thus strongly favored by the creation of lipid packing defects such as those introduced by high membrane curvature. Site-directed mutagenesis reveals that hydrophobic residues in the ALPS motif are indeed critical for the association of ArfGAP1 with model liposomes, for its activity toward membrane-bound Arf1-GTP as well as for its Golgi localization (*16*, *18*). Moreover, replacing S/T residues in the polar face with basic residues makes the ALPS motif much less sensitive to membrane curvature for its adsorption to negatively charged liposomes (G. Drin, personal communication).

Here we report that ArfGAP1 contains a second motif that, despite an amino acid sequence quite distant from the originally described ALPS motif, shares the same general physicochemical properties. This second ALPS motif also forms an amphipathic α-helix at the surface of highly curved liposomes and contributes together with the first ALPS motif to the recognition of membrane curvature by ArfGAP1.

MATERIALS AND METHODS

Protein Expression and Purification. All point mutations were introduced using the Quik-Change site-directed mutagenesis kit (Stratagene). The full-length sequence of rat ArfGAP1 (residues 1–415) with silent mutations for expression in *Escherichia coli* (*8*) was PCR amplified and cloned into the pET16b vector (Novagen) between NdeI and BamHI sites. The protein was expressed in *E. coli* and purified from inclusion bodies as described for the construct of residues 1–257 (*16*). Fragments of ArfGAP1 in a fusion with GST

were cloned in a pGEX-2T expression vector (Pharmacia), which includes a thrombin cleavage site. For protein purification, transformed bacteria were resuspended in 50 mM Tris (pH 7.4) and 150 mM NaCl (TN buffer), supplemented with 1 mM PMSF, 1 μM pepstatin, 10 μM bestatin, 10 μM phosphoramidon, and a cocktail of anti-proteases (Roche) and broken with a French press. The supernatant was incubated for 1 h with glutathione−Sepharose 4B beads (Amersham). The beads were washed three times with TN buffer, and the GST fusions were eluted in the same buffer supplemented with 10 mM glutathione. Alternatively, the beads were incubated with thrombin to allow the elution of the ArfGAP1 peptides. The peptides were further purified by HPLC on a Chromolith C18 column (Merck) with an acetonitrile gradient. The peptide identity was checked by mass spectrometry. The ArfGAP1 peptides were lyophilized and stored at −20 °C before being used.

NBD Labeling. The ALPS1 peptide (residues 192−257) and the ALPS1−ALPS2 peptide (residues 192−304), both carrying the A236C mutation, were resuspended in 50 mM Hepes (pH 7.2) and 120 mM potassium acetate (HK buffer) at a final concentration between 40 and 200 μM. A 10-fold molar excess of *N*,*N*′-dimethyl-*N*-(iodoacetyl)-*N*′-(7-nitrobenz-2-oxa-1,3-diazol-4-yl)ethylenediamine (IANBD amide, Molecular Probes) in dimethylformamide (stock solution at 5 mM) was added, and the mixture was incubated at room temperature for 90 min. The reaction was stopped by the addition of 10 mM dithiothreitol. The sample was further purified on a Chromolith C18 column (Merck) using an acetonitrile gradient. Labeled products were detected by measuring the absorbance at three wavelengths (220, 280, and 478 nm) followed by SDS−PAGE analysis and direct visualization of the gel in a fluorescence imaging system (LAS 3000, Fuji). The identity of the labeled peptides was confirmed by mass spectrometry.

Liposomes. Lipids in chloroform were purchased from Avanti Polar Lipids except egg PC (Sigma) and NBD-PE (Molecular Probes). A lipid film containing (mole percent) egg PC (50), liver PE (19), brain PS (5), liver PI (10), cholesterol (16), and, when indicated, NBD-PE (0.2) was prepared by evaporation. The film was resuspended in HK buffer. After five steps of thawing and freezing in liquid nitrogen, the liposome suspension was extruded sequentially through (pore size) 0.4, 0.2, 0.1, 0.05, and 0.03 μm polycarbonate filters using a hand extruder (Avanti). Alternatively, very small liposomes were prepared by sonication with a titanium tip sonicator (Misonix). Titanium and lipid debris were removed by centrifugation at 100000*g* for 20 min to produce a homogeneous population of liposomes. The liposome radius was estimated by dynamic light scattering (DLS) using a Dyna Pro instrument. Liposomes were stored at room temperature and used within 2 days.

Flotation Experiments. Proteins (0.5−1 μM) and NBD-labeled liposomes (0.5−1 mM) were incubated in 50 mM Hepes (pH 7.2), 120 mM potassium acetate, and 1 mM MgCl$_2$ (HKM buffer) at room temperature for 5 min in a total volume of 150 μL. The suspension was then adjusted to 30% (w/v) sucrose and overlaid with 200 μL of HKM buffer containing 25% (w/v) sucrose and with 50 μL of HKM buffer containing no sucrose. The sample was centrifuged at 240000*g* in a Beckman swing rotor (TLS 55) for 1 h. The 100 μL top fraction was collected manually using a Hamilton

syringe and analyzed by SDS−PAGE using Sypro-orange staining (Molecular Probes). The gels were visualized in a FUJI LAS-3000 fluorescence imaging system.

GTPase Measurements. The activity of ArfGAP1 on Arf1 was measured by a tryptophan fluorescence assay (*20*). The experiments were performed in a cylindrical quartz cuvette (600 μL) equilibrated at 37 °C and equipped with a magnetic bar for continuous stirring. Tryptophan fluorescence was measured at 340 nm (bandwidth of 10 nm) upon excitation at 297.5 nm (bandwidth of 1.5 nm) in a Shimadzu RF-5301-PC spectrofluorometer. The cuvette initially contained liposomes of a defined size (200 μM lipids) in HKM buffer. At the indicated times, myristoylated Arf1-GDP (0.5 μM), GTP (50 μM), and EDTA (2 mM) were sequentially added to promote the replacement of GDP with GTP. When nucleotide exchange was complete, 2 mM $MgCl_2$ was added, followed by the addition of ArfGAP1 (50 nM) to initiate GTP hydrolysis.

Tryptophan Fluorescence Measurements of the Partitioning of ALPS Peptides on Liposomes. To assess the binding of the various ArfGAP1 peptides to liposomes, the decrease in tryptophan fluorescence at 370 nm of a solution containing 1 μM peptide in HK buffer was measured upon stepwise additions of sonicated liposomes from a concentrated stock solution. The experiments were performed at 37 °C in a cylindrical quartz cuvette while the sample was continuously stirred. The added liposomes scattered light and slightly diluted the sample. To correct for these effects, two control experiments were performed (*21*), one in which the liposomes were added to the buffer and a second in which the liposomes were added to a solution of tryptophan in the zwitterionic form, which remains soluble. After i additions of liposomes, the fluorescence levels in the experiments with the peptide, with the buffer, and with tryptophan are F_i, L_i, and W_i, respectively.

The specific fluorescence change due to liposome binding is

$$\Delta F_i = (F_i - L_i)[W_0/(W_i - L_i)] - F_0 \qquad (1)$$

This change is proportional to the amount of liposome-bound peptide:

$$\Delta F = f[P_m] \qquad (2)$$

The following equation describes the partitioning of a peptide between the aqueous phase and the liposome surface:

$$[P_m] = ([P_t][L])/(K_p + [L]) \qquad (3)$$

where $[P_t]$ is the total concentration of peptide, $[P_m]$ is the concentration of peptide that is bound to the lipid membrane, and $[L]$ is the concentration of lipids that is accessible to the peptide. When the liposomes are monolamellar and when the concentration of lipids is large enough that the liposome surface covered by the peptide can be neglected compared to the total liposome surface, $[L]$ can be estimated as approximately one-half of the total lipid concentration (0.5-$[L_t]$) because only the outer monolayer is accessible. Because very small liposomes were used in these titration experiments ($R_h = 25$ nm), there is a slight excess of lipids in the outer leaflet, and therefore, a better approximation is $[L] = 0.55$-$[L_t]$. Thus, one obtains

$$[P_m] \approx (0.55[P_t][L_t])/(K_p + 0.55[L_t]) \qquad (4)$$

K_p is a partition coefficient and is expressed in molar. It should not be considered as a true equilibrium constant for the binding of one peptide for one lipid but simply reflects the concentration of exposed lipids at which 50% of the peptide is bound to the liposome surface (*22*). This experimental partition coefficient can be converted into K_p', a dimensionless coefficient, which directly reflects the preference of the peptide for the lipid phase compared to the water phase ($K_p' = [H_2O]/K_p$). Thus, if $K_p = 1$ mM, $K_p' = 55\,500$, meaning that the peptide has a 55500-fold preference for the lipid phase compared to the bulk water phase.

When a peptide adsorbs significantly at low lipid concentrations, the approximation $[L] \approx 0.55[L_t]$ is no longer valid because bound peptides occupy a large fraction of the liposome surface. In that case, it is easier to consider a scheme where each bound peptide occupies a membrane patch consisting of n lipids with an apparent equilibrium constant, K_d (*23*):

$$P + L_n \overset{K_d}{\leftrightarrow} PL_n$$
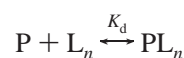
The corresponding quadratic equation is

$$[P_m] = [PL_n] = 0.5\{[P_t] + 0.55[L_t]/n + K_d - [([P_t] +$$
$$0.55[L_t]/n + K_d)^2 - 2.2[P_t][L_t]/n]^{1/2}\} \quad (5)$$

Note that $K_p = nK_d$ and $K_p' = [H_2O]/(nK_d)$.

Equations 4 and 5 with the proportionality factor (*f*) are used to fit the data. Equation 4 is used for peptides having a low avidity for membranes as it has only two parameters (K_p and f). When eq 4 fails to fit the data, eq 5 is used, giving three parameters, K_d, n, and f.

NBD Fluorescence. NBD-labeled ALPS peptides (1 μM) were incubated at 37 °C with Golgi-mix liposomes (600 μM) of defined radius in HK buffer supplemented with 1 mM DTT. Emission fluorescence spectra were measured from 520 to 680 nm (bandwidth of 5 nm) upon excitation at 505 nm (bandwidth of 5 nm) in a small quartz cell (total volume of 100 μL). Control spectra were acquired in the absence of peptide to subtract the light scattering signal from the liposomes. The corrected fluorescence intensity at 529 nm was plotted as a function of liposome radius.

CD Spectroscopy. Lyophilized peptides were resuspended in 10 mM Tris (pH 7.5) and 150 mM KCl and ultracentrifuged to eliminate aggregates. The absorbance at 280 nm was used to determine the peptide concentration in the supernatant. CD measurements were performed at room temperature in a quartz cell with an optical path length of 0.05 cm. Spectra were recorded on a Jasco J-815 spectrometer at a scan speed of 50 nm/min and with a bandwidth of 1 nm. The spectra that are shown are the average of two to four recordings and were corrected for the buffer or liposome background. Secondary structure analysis was performed using three methods: SELCON3, CONTILL, and CDSSTR (*24*).

Cell Transfection and Fluorescence Microscopy. The procedures that were employed have previously been described (*18*). Briefly, ArfGAP1 (residues 143−415) and mutants thereof were cloned into eGFP-C2 (Clontech). The
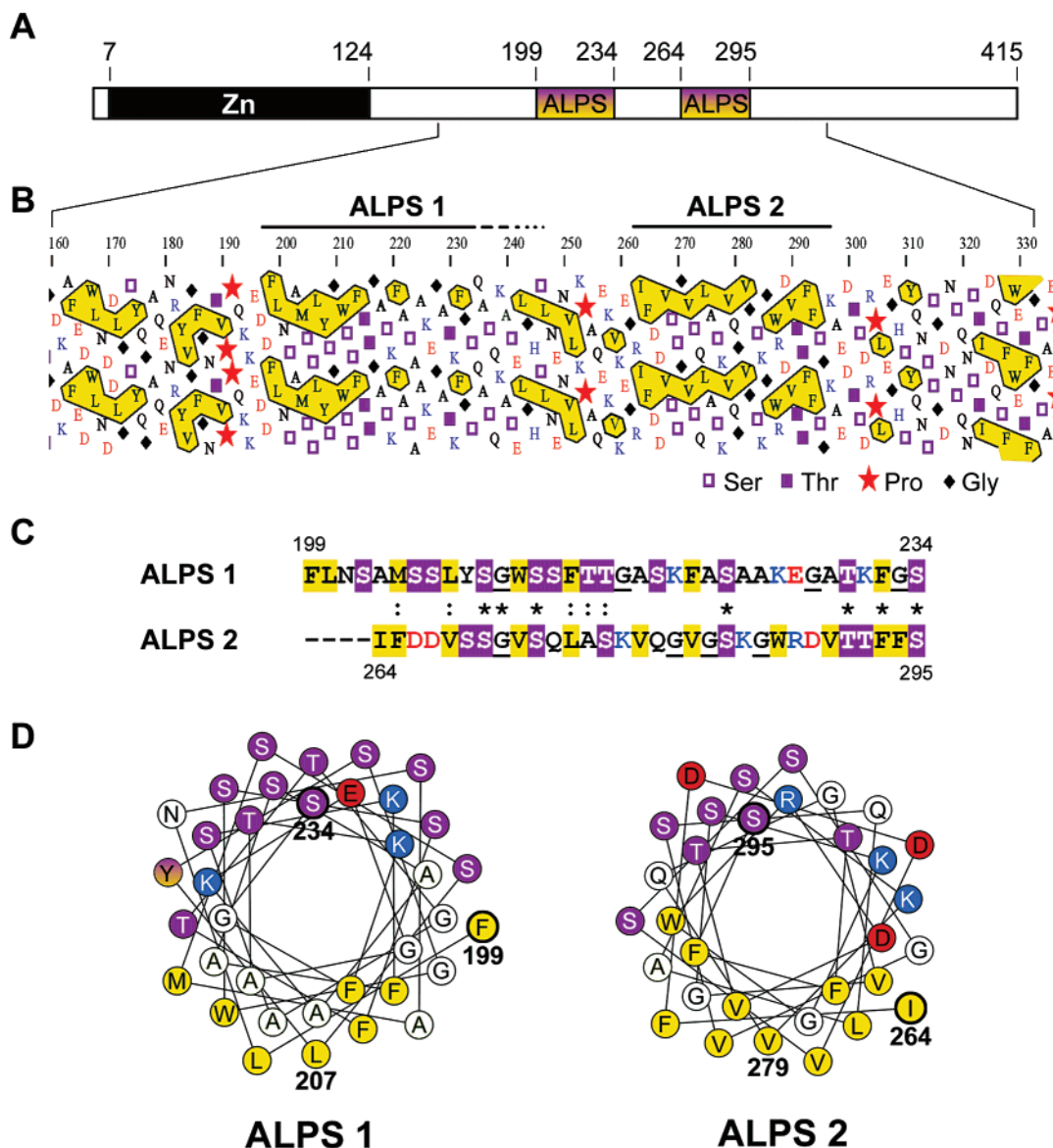
FIGURE 1: Identification of a second putative ALPS motif in the ArfGAP1 sequence. (A) Localization of the ALPS1 and ALPS2 motifs in ArfGAP1. (B) HCA plot of the central region of ArfGAP1. The primary sequence is written along parallel and nearly vertical lines and is duplicated. P, G, S, and T residues are represented by symbols as indicated. Yellow areas represent hydrophobic clusters (F, I, L, M, V, W, and Y). A horizontal cluster is indicative of an α-helix as this corresponds to the regular spacing of hydrophobic residues every three or four residues. The ALPS1 and ALPS2 motifs include such a cluster and are also characterized by the abundance of S and T residues (mauve squares). (C) Sequence alignment of ALPS1 and ALPS2 obtained with Clustal W. Note the low level of amino acid identity. (D) Projections of the ALPS1 and ALPS2 motifs on a helical wheel. The resemblance between the two motifs is obvious in this representation: the segregation between S/T residues (mauve) and hydrophobic residues (yellow). Basic and acidic residues are colored blue and red, respectively. The hydrophobic residues that have been mutated into Asp in this study are denoted.

GFP fusions were transfected into HeLa cells and visualized 24 h later under a Leica DMIRE2 inverted fluorescence microscope at a 40× magnification.

RESULTS

Identification of a Second Putative ALPS-like Motif in the ArfGAP1 Sequence. Using HCA [Hydrophobic Cluster Analysis (http://bioserv.rpbs.jussieu.fr/RPBS)], which highlights the regular distribution of hydrophobic residues in protein sequences and is used to predict the propensity of a region to form secondary structures (*25*), we noticed that, despite a low level of amino acid identity, the region between I264 and S295 of ArfGAP1 shows some similarities with the ALPS motif, defined as F199–S234 (Figure 1A–C). Three points are noteworthy. First, both sequences exhibit a

regular distribution of hydrophobic residues with a periodicity of three to four amino acids, a feature suggestive of an amphipathic α-helical structure as illustrated by helical-wheel projections (Figure 1D). Second, among the polar residues that are intercalated between the hydrophobic residues, many are Ser and Thr residues. In contrast, basic and acidic residues are rare. Consequently, the polar face of the putative α-helix should be weakly charged (Figure 1D). Third, both sequences contain several glycine residues (*n* = 4), which should favor structural flexibility and notably a switch from a random coil to an α-helix conformation. We demonstrated previously that such a conformational change is coupled to the adsorption of the ALPS motif to highly curved membranes (*16*). In the following, we will refer to the new region as ALPS2, whereas the original ALPS motif will be called ALPS1.
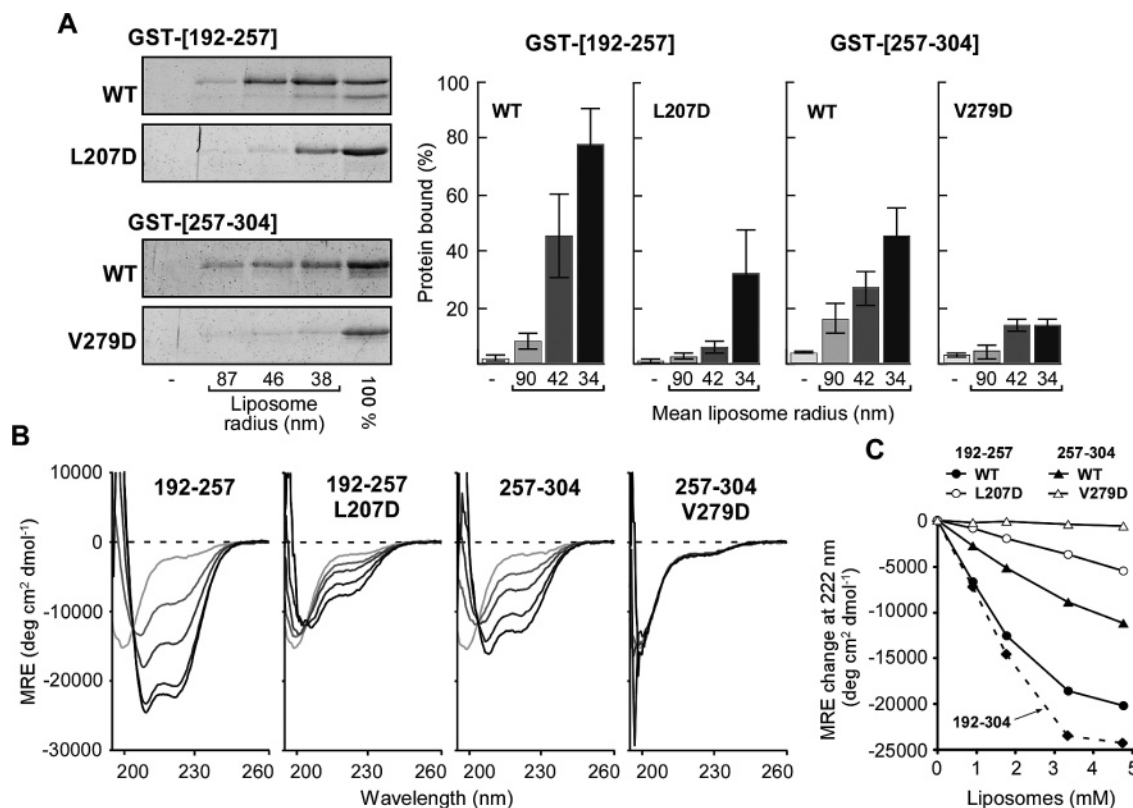
FIGURE 2: Binding and folding of the ALPS1 and ALPS2 motifs on model liposomes of a defined size. (A) For flotation experiments, GST constructs (0.75 μM) containing the ALPS1 or ALPS2 motif of ArfGAP1 were incubated with Golgi-mix liposomes (0.75 mM lipids) of a defined size or with no liposome. When indicated, a residue in the hydrophobic face of the putative α-helix was replaced with an Asp residue (see Figure 1D). Liposome-bound proteins were recovered at the top of sucrose cushions and analyzed by SDS−PAGE (left panels). The 100% lane was used to determine the protein ratio in the top fraction. The right panels show the quantification ($\pm$standard error) of four independent experiments using different batches of liposomes. (B) Far-UV CD spectra of the ALPS1 and ALPS2 peptides (40 μM) in solution or with increasing concentrations of small DOPC/DOPS (70:30) liposomes ($R_h = 16 \pm 7$ nm) obtained by sonication. From the lightest to the darkest curves, the lipid concentration was 0, 1.9, 1.75, 3.33, and 4.75 mM. Note the well-defined isodichroic point at 203 nm, which suggests a simple two-state equilibrium between a random-coil conformation in solution and an α-helical conformation on liposomes. (C) Change in mean residue ellipticity (MRE) at 222 nm as a function of lipid concentration for the four peptides that were tested. Also shown are the results obtained with the ALPS1−ALPS2 peptide [residues 192−304 (- - -)].

Membrane Partitioning and Folding of the Isolated ALPS2 Motif. To determine if the ALSP2 motif can act as a sensor of membrane curvature, we expressed and purified the fragment of residues 257−304 of ArfGAP1 in a fusion with GST (GST−ALPS2) and assessed its avidity for liposomes of a defined size by a flotation assay. As a control, the same experiment was carried out with GST−ALPS1 (residues 192−257 of ArfGAP1). The liposomes contained a mixture of lipids that mimics the Golgi composition (Golgi-mix) and were calibrated in size by extrusion through polycarbonate filters of a defined pore size (from 400 to 30 nm). With this method, we could vary the average liposome radius from 130 to 30 nm as estimated by dynamic light scattering (DLS). The protein was mixed with liposomes at a protein:lipid molar ratio of 1:1000, and the liposomes were then recovered at the top of sucrose cushions by ultracentrifugation. The fraction of liposome-bound protein was quantified by SDS−PAGE using the fluorescent dye Sypro-orange.

As shown in Figure 2A, GST−ALPS2 bound to Golgi-mix liposomes and exhibited a preference for small ($R_h = 38$ nm) versus large ($R_h = 87$ nm) liposomes. This suggests that ALPS2 can function, like ALPS1, as a sensor of membrane curvature. However, as compared to GST−ALPS1, less protein was recovered in the liposome fraction, suggesting that ALPS2 has less avidity for lipid membranes

than ALPS1. In addition, the dependency on liposome size was not as sharp as that observed for ALPS1.

Next, we used CD spectroscopy to determine the secondary structure of the ALPS2 peptide (residues 257−304) either in solution or bound to liposomes. A first CD spectrum of the peptide was recorded in buffer followed by measurements at increasing concentrations of small DOPC/DOPS liposomes made by sonication. As judged from the disappearance of the minimum at 200 nm and the appearance of two minima at 208 and 222 nm, the ALPS2 peptide, like ALPS1, switches from a random coil structure in solution to an α-helix conformation once bound to liposomes (Figure 2B). Plotting the mean residue ellipticity (MRE) at 222 nm against lipid concentration (Figure 2C) suggested, however, that ALPS2 has less avidity for lipid membranes than ALPS1, in agreement with the results of the flotation assay.

Because of their amphipathic nature, the α-helices formed by ALPS1 and ALPS2 should lie parallel to the lipid bilayer with the nonpolar face embedded in the hydrocarbon core of the membrane. Thus, replacing one hydrophobic residue in the nonpolar face of ALPS1 or ALSP2 with a negatively charged amino acid should strongly perturb the membrane partitioning and folding of these peptides. L207D and V279D mutations were introduced into the ALPS1 and ALPS2 constructs, respectively. As expected, the V279D mutation

nearly abolished the adsorption of GST−ALPS2 regardless of liposome size (Figure 2A). Moreover, the addition of small liposomes to the corresponding mutated ALPS2 peptide induced no increase in helicity (Figure 2B). The L207D mutation in the ALPS1 motif had a less drastic effect. First, substantial binding of GST−ALPS1[L207D] to small liposomes could be detected (Figure 2A). Second, a clear increase in the helicity of the corresponding mutated peptide was observed upon addition of sonicated liposomes (Figure 2B). However, plotting the change in ellipticity at 222 nm against lipid concentration suggests that the mutation markedly weakens the avidity of the ALPS1 peptide for lipid membranes as no saturation of the CD signal could be observed within the range of liposomes used in the experiments, in contrast to what was observed with the wild-type form (Figure 2C).

Taken together, the experiments shown in Figure 2 suggest that ArfGAP1 contains two motifs, ALPS1 and ALPS2, of ~35 amino acids that share similar physicochemical properties. These motifs show no well-defined structure in solution but adopt an α-helical conformation at the surface of lipid membranes. Furthermore, the partitioning−folding process is favored by reducing the size of the liposomes, suggesting that each motif can act as a sensor of membrane curvature. However, for a given liposome radius, it seems that the ALPS1 motif adsorbs more readily than the ALPS2 motif.

The ALPS2 Motif Contributes to the Golgi Localization of ArfGAP1. Having demonstrated that the isolated ALPS2 motif can act as a sensor of membrane curvature, we tested its functionality in vivo. It was shown previously that point mutations of conserved hydrophobic residues in the ALPS1 motif redistribute ArfGAP1 from the Golgi to the cytosol, thus providing the first in vivo evidence of the importance of the ALPS1 motif in the localization of ArfGAP1 (*18*). Furthermore, the effects observed for several mutations were compatible with a model in which the ALPS1 motif directly interacts with the lipid membrane through hydrophobic interactions (*18*). However, it was also noticed that the ALPS1 motif is not sufficient for Golgi targeting since the minimal construct that shows Golgi localization encompasses residues 203−334 and thus includes both ALPS motifs (*17, 18*). In addition, deletion of residues 259−280 was found to abrogate Golgi localization, pointing to a possible role of ALPS2 in this process (*18*). To test this possibility, we assessed the effect of the V279D mutation, which essentially abolished the binding of the isolated ALPS2 motif to liposomes (Figure 2), on the subcellular distribution of the noncatalytic region of ArfGAP1 (residues 143−415). In agreement with previous studies, the noncatalytic region of ArfGAP1, which was fused on its N-terminus to the carboxy terminus of GFP, showed a strong perinuclear staining, which is characteristic of the Golgi apparatus (*17, 18*). In contrast, the V279D mutant exhibited more diffuse localization, indicating a significant decrease in its level of interaction with the Golgi (Figure 3). Other Asp mutations of hydrophobic residues within the ALPS2 sequence (W287D and V290D) also caused a strong decrease in the level of ArfGAP1 Golgi localization (data not shown). Thus, the ALPS2 motif contributes to the Golgi targeting of ArfGAP1.

The ALPS2 Motif Contributes to the Sensitivity of ArfGAP1 to Membrane Curvature. Next we wished to determine the contribution of the ALPS2 motif to the sensitivity of
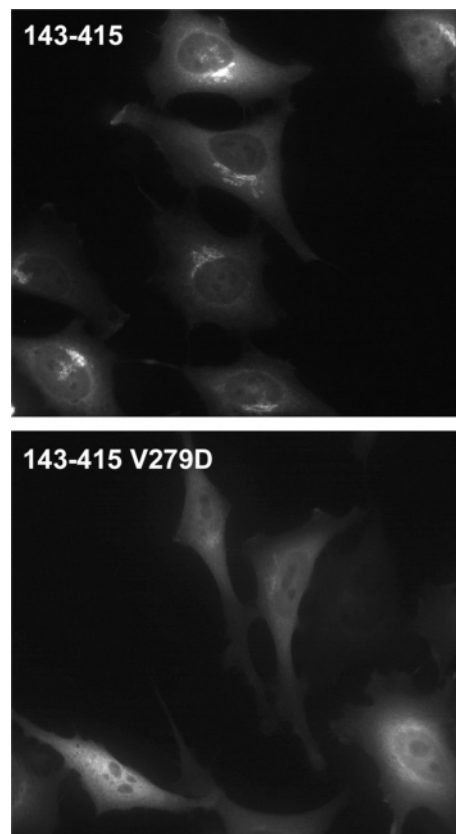

FIGURE 3: ALPS2 contributes to the Golgi localization of ArfGAP1. The noncatalytic region of ArfGAP1 (residues 143−415) fused to GFP was transiently expressed in HeLa cells. The V279D single mutation in the ALPS2 motif causes a strong reduction in the level of perinuclear localization.

ArfGAP1 to membrane curvature in vitro. For this, the L207D and/or the V279D mutations, which perturb the membrane partitioning of the isolated ALPS1 and ALPS2 motifs, respectively (see Figure 2A), were introduced in full-length ArfGAP1. The various ArfGAP1 proteins containing a hexahistidine tag at the N-terminus were purified by nickel chromatography followed by MonoQ chromatography. The wild-type form and the three mutants (L207D, V279D, and L207D/V279D) exhibited similar background GAP activity in solution on a soluble form of Arf1-GTP (Δ17-Arf1), suggesting that the catalytic machinery residing in the N-terminal part was not affected by the mutations (data not shown).

Figure 4A shows that the L207D mutation and the V279D mutation caused a significant decrease in the level of adsorption of ArfGAP1 to Golgi-like liposomes, which remained however sensitive to liposome size. Importantly, combining the two mutations caused a more severe defect, suggesting that adsorption of ArfGAP1 to lipid membranes is governed by both motifs. It should be noted, however, that ArfGAP1[L207D/V279D] exhibits residual binding to small liposomes, which may be due to the fact that the L207D mutation does not completely abolish the binding of the ALPS1 motif to membranes (see Figure 2A).

The contribution of the two ALPS motifs was confirmed by measuring the GAP activity of the various mutants on liposome-bound Arf1-GTP (Figure 4B). GTP hydrolysis in Arf1 can be readily followed by tryptophan fluorescence because of the large difference between the fluorescence of
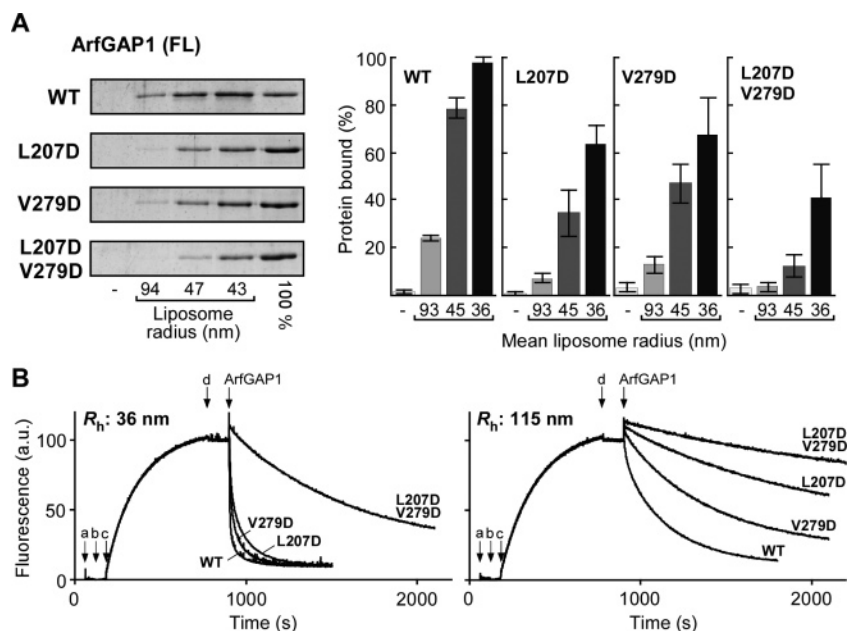
FIGURE 4: Synergy between the ALPS1 and ALPS2 motifs for the membrane adsorption of ArfGAP1 and its activity on Arf1-GTP. (A) Flotation experiments. Full-length ArfGAP1 carrying the indicated mutations in ALPS1 and/or ALPS2 was incubated with Golgi-mix liposomes of a defined size or with no liposome. Liposome-bound proteins were recovered at the top of sucrose cushions. The left panel shows the SDS−PAGE of a typical experiment. The right panels compile the results of two independent experiments using different batches of liposomes. (B) GAP assay. Arf1-GDP (injection a) was first incubated with small (left) or large (right) liposomes and converted to the GTP-bound form by the addition of an excess of GTP (b) and by the addition of 2 mM EDTA (c, giving 1 μM free Mg^{2+}). Thereafter, an excess of $MgCl_2$ was added (d), and GTP hydrolysis was initiated by the addition of 50 nM ArfGAP1 bearing the indicated mutations.

Arf1-GTP (high fluorescence) and Arf1-GDP (low fluorescence). With small liposomes (R_h = 36 nm), where the time course of GTP hydrolysis induced by wild-type ArfGAP1 was very fast ($t_{1/2}$ = 6 s), the L207D mutation and the V279D mutation caused modest decreases in the rate of GTP hydrolysis ($t_{1/2}$ = 29 and 15 s, respectively). However, when the two mutations were combined, GTP hydrolysis was dramatically slowed ($t_{1/2}$ = 558 s). This apparent synergy between the two mutations was also observed with large liposomes (R_h = 115 nm), where the rate of GTP hydrolysis induced by wild-type ArfGAP1 was very slow ($t_{1/2}$ = 99 s). However, in that case, the effect of the individual mutations was more pronounced.

Quantitative Analysis of the Contribution of ALPS1 and ALPS2 to Membrane Adsorption. Having established that both ALPS motifs contribute to the binding of full-length ArfGAP1 to lipid membranes, we wished to study in a more quantitative manner the synergy between the two motifs. For this, we used spectroscopic assays by which one can compare the lipid binding properties of the individual ALPS peptides (residues 192−257 and residues 257−304) with that of a construct including the two motifs in tandem (residues 192−304).

We first took advantage of the fact that each ALPS motif carries a tryptophan residue (W211 in ALPS1 and W287 in ALPS2), which should experience a change in environment upon membrane binding and thus act as an intrinsic fluorescence probe of this event. Figure 5A shows the emission spectra of the ALPS1, ALPS2, and ALPS1−ALPS2 peptides in the absence or presence of sonicated liposomes (R_h = 24 ± 12 nm). In all cases, a blue shift was observed, suggesting that the tryptophan groups are shifted from an aqueous environment to a nonpolar environment. The fluorescence decrease at 370 nm was then plotted as a function of lipid concentration to determine the partition coefficient of the peptides (filled symbols in Figure 5B). For ALPS1, we could fit the data with a hyperbolic function giving an apparent partition coefficient (K_p) of ca. 290 μM lipid. For ALPS2, we could have only a rough estimate of the partition coefficient since the fluorescence change showed no saturation within the range of lipid concentrations that was used (K_p in the millimolar range). Strikingly, the fluorescence change observed for the ALPS1−ALPS2 peptide was markedly different from that observed for the individual ALPS peptides. First, at any lipid concentration, the decrease in intensity was larger than the sum of the decreases measured for ALPS1 and ALPS2. Second, the dose−response curve showed a sharp shape with a saturation at lipid concentrations of >250 μM, which contrasted with the smoother dose−response curves observed for the individual ALPS peptides. This suggested that the ALPS1−ALPS2 peptide has a much higher avidity for the lipid membrane than the isolated ALPS motifs. For the ALPS1−ALPS2 peptide, we could not fit the data with a classical hyperbolic function because the concentration of free lipid, which should be used in this equation, can no longer be approximated by the total lipid concentration. In other words, we have to take into account the fact that each bound peptide occupies a membrane patch of n lipids that is no longer available for the binding of other peptides (see Materials and Methods). Fitting the fluorescence change by a quadratic equation indicates that the ALPS1−ALPS2 peptide binds to a membrane patch of 108 (n) lipids with an apparent affinity (K_d) of 0.067 μM. This gives for the corresponding partition coefficient (K_p) a value of 108 × 0.067 = 7 μM. Compared to values of 290 μM for ALPS1 and ca. 1 mM for ALPS2, this indicates that the combination of ALPS1 and ALPS2 results in a 40−100-fold increase in membrane binding.
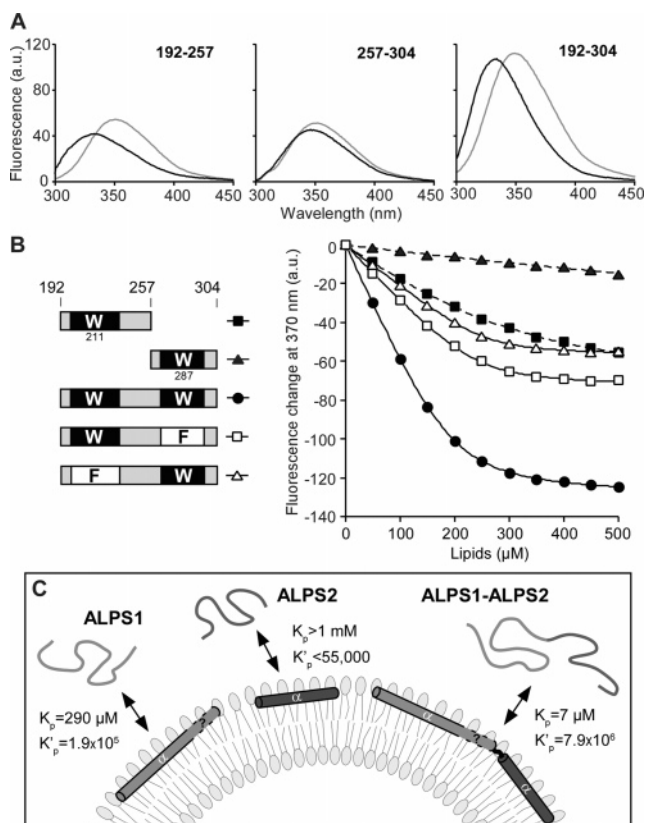
FIGURE 5: Quantitative measurements of the affinity of the ALPS motifs for small liposomes by tryptophan fluorescence. (A) Fluorescence emission spectra of the ALPS1, ALPS2, and ALPS1−ALPS2 peptides (1 μM) in buffer (gray traces) and after the addition of small Golgi-mix liposomes (500 μm) obtained by sonication [R_h = 25 nm (black traces)]. The corresponding blank spectra (buffer alone or liposomes alone) have been subtracted, and a scale factor, calculated from an experiment with tryptophan in the zwitterionic form, was applied to the spectra observed in the presence of liposomes to correct for the loss of excitation and emission light by scattering. (B) Corrected fluorescence change at 370 nm induced by the stepwise addition of sonicated liposomes to the indicated peptides, which are schematized at the left. The solid lines are quadratic fits, whereas the dashed lines are hyperbolic fits (see Materials and Methods). (C) Schematic view of the results. The membrane (thickness and curvature) and the helices are shown approximately to scale. The partition coefficients (K_p) have been estimated from the fits shown in panel B. K_p can be converted into K_p', a dimensionless coefficient, which directly reflects the preference of the peptide for the liposome surface compared to the water phase.

Both W211 in ALPS1 and W287 in ALPS2 should contribute to the overall fluorescence signal observed for the ALPS1−ALPS2 peptide. To estimate their relative contribution, we prepared two mutated forms of the ALPS1−ALPS2 peptide in which either W211 or W287 was replaced with phenylalanine. We reasoned that a W to F mutation should have a minor impact on membrane adsorption but would make the corresponding ALPS motif "silent" in terms of fluorescence. Figure 5B shows that the fluorescence changes observed for the mutated ALPS1−ALPS2 peptides were approximately one-half of those observed for the wild-type form but that the shape of the dose−response curves was very similar. Quadratic fits give indeed very similar values of K_d and n. Therefore, we conclude that W211 in ALPS1 and W287 in ALPS2 contribute approximately equally to the fluorescence change observed for the ALPS1−ALPS2

peptide. Interestingly, the Phe mutants allow a better observation of the synergy between the two ALPS motifs. This can be seen by comparing the fluorescence changes observed for ALPS2 (▲) and for the ALPS1[W211F]−ALPS2 peptide (△) in Figure 5B. In both cases, W287 of the ALPS2 motif is solely responsible for the fluorescence signal, yet W287 partitions weakly in the bilayer when present in isolated ALPS2 but much more efficiently when ALPS1 was linked to ALPS2. This suggests that the partitioning of ALPS1 on lipid membranes greatly facilitates the partitioning of ALPS2. The same reasoning can be made by comparing ALPS1 with ALPS1−ALPS2[W287F] peptides.

The synergy between the two ALPS motifs was confirmed by CD spectroscopy. Titration experiments similar to that shown in Figure 2B for the individual ALPS peptides were performed with the ALPS1−ALPS2 peptide, and the results are compiled in Figure 2C (dashed line). If there was no synergy between the ALPS1 and ALPS2 motif for their folding onto small liposomes, the MRE value of the ALPS1−ALPS2 peptide should be between the values observed for the individual ALPS1 and ALPS2 peptides. In contrast, at any lipid concentration, the MRE value at 222 nm was even more negative than that observed for ALPS1, hence confirming a mutual help between the two ALPS motifs for their folding and/or adsorption at the liposome surface (Figure 2C). In the presence of 4.75 mM DOPC/DOPS sonicated liposomes, the α-helical content of the ALPS1−ALPS2 peptide was estimated to be 80% compared to 65% for ALPS1 and 36% for ALPS2.

Estimation of the Contribution of ALPS2 to the Response to Membrane Curvature. Tryptophan fluorescence is a convenient way to follow the binding of ALPS peptides to small liposomes. However, it was difficult to perform similar experiments using liposomes of larger size as they strongly scattered UV light. To circumvent this, we used an extrinsic fluorescence probe, NBD, which, like tryptophan, shows a blue shift in its emission spectrum upon moving from a polar to a nonpolar environment, but absorbs and emits in the visible spectrum where the contribution of light scattering by large liposomes is small. To attach NBD covalently, we replaced Ala236 in ALPS1 and in the ALPS1−ALPS2 peptide with a cysteine. Ala236 is at the C-terminus of the ALPS1 motif, and a NBD group at this position should experience a change in environment when the peptide adsorbs and folds at the membrane surface.

The fluorescence emission spectra of ALPS1-NBD and ALPS1-NBD−ALPS2 peptides were recorded in solution or in the presence of Golgi-mix liposomes (600 μM) of decreasing size. Figure 6 shows that when incubated with large Golgi-mix liposomes (R_h = 120 nm), both peptides exhibited an emission spectrum close to that observed in solution, suggesting that they remained essentially soluble. However as the liposome size decreases, a sharp increase in NBD fluorescence was observed, further illustrating that ALPS motifs function as acute sensors of membrane curvature. Importantly, the peptides did not respond to the same range of membrane curvature: the response of the ALPS1−ALPS2 peptide to the radius of the liposomes was shifted by about +20 nm as compared to the response of the ALPS1 peptide. This suggests that the presence of ALPS2 in tandem with ALPS1 is not required for the detection of
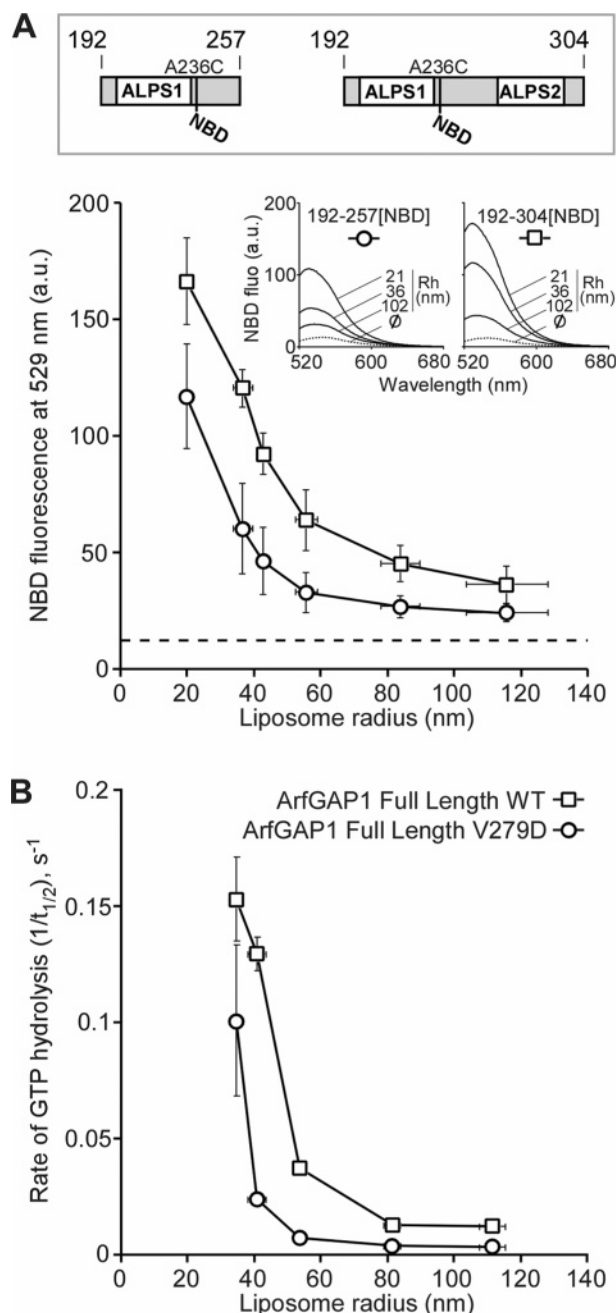
FIGURE 6: ALPS2 modulates the response of ArfGAP1 to membrane curvature. (A) NBD fluorescence assay. The constructs are schematized. The insets show typical emission spectra of NBD-labeled ALPS1 and ALPS1−ALPS2 peptides in solution (dashed curves) or in the presence of Golgi-mix liposomes of a defined radius. The fluorescence intensity at 529 nm was plotted as a function of liposome radius. The data shown are from five independent experiments. The horizontal and vertical bars show the standard deviation of the liposome hydrodynamic radius and of the NBD fluorescence intensity, respectively. The horizontal dashed line indicates the fluorescence level of the NBD peptides in solution. (B) GAP assay. GTPase measurements similar to those shown in Figure 4B were performed with Golgi-mix liposomes of a defined radius and loaded with Arf1-GTP. GTP hydrolysis was initiated by the addition of 50 nM ArfGAP1 (wild-type or V279D). The half-time ($t_{1/2}$) of GTP hydrolysis was determined graphically from the tryptophan fluorescence decay. The plot shows the rate ($1/t_{1/2}$) ± the variation of GTP hydrolysis as a function of liposome radius for two independent experiments.

membrane curvature per se but tunes this detection toward larger radii (lower level of curvature).

We compared the results of the NBD fluorescence assay with GAP activity measurements performed with the wild-type form of ArfGAP1 and with the V279D mutant. As this mutation abolished the binding and/or folding of the isolated ALPS2 motif (Figure 2), a mutant bearing this mutation should rely only on ALPS1 for its interaction with lipid membranes, and its behavior in the GAP assay was thus expected to match the behavior of the ALPS1 peptide in the NBD fluorescence assay. In contrast, the sensitivity to membrane curvature of wild-type ArfGAP1, with two functional ALPS motifs, should better fit with the behavior of the ALPS1−ALPS2 peptide in the NBD fluorescence assay. Figure 6B reports the rate of Arf1-GTP hydrolysis catalyzed by wild-type ArfGAP1 or by the V279D mutant on Golgi-mix liposomes with various radii. Clearly and as expected, the V279D mutation does not abolish the sensitivity to membrane curvature but shifts the response to shorter radii. Thus, one can estimate that when the ALPS2 motif is made nonfunctional by the V279D mutation, the threshold for the response of the GAP activity to membrane curvature is shifted to an R of ≈60 nm, compared to an R of ≈80 nm for the wild-type form. Taken together, the NBD fluorescence assay and the GAP assay suggest that the engagement of two ALPS motifs versus one determines the range of curvature at which ArfGAP1 responds. It should be noted, however, that the response of full-length ArfGAP1 to membrane curvature (as judged from the GAP assay) was even sharper than that observed for the ALPS1−ALPS2 peptide measured by the NBD fluorescence assay. As proposed for other members of the ArfGAP family (*26*), intramolecular interactions within the entire ArfGAP1 molecule affecting the availability of the ALPS motifs and/or the activity of the catalytic Zn-finger fold could explain this difference.

Adaptation to Lipid Membranes with Different Lipid Compositions. ArfGAP1 is sensitive not only to membrane curvature but also to the geometry of lipids (*11−13, 19*). This dual sensitivity has the same cause: the ALPS motifs adsorb preferentially on membranes that display defects in lipid packing because such defects facilitate the insertion of hydrophobic residues. Therefore, a conical lipid in a flat membrane is somehow equivalent to a cylindrical lipid in the outer leaflet of a curved membrane: the mismatch between the lipid geometry and the actual curvature of the membrane leaves some space for the insertion of hydrophobic residues. We reasoned that depending on the lipid composition and notably the average level of acyl chain unsaturation, there could be an advantage of having one or two functional ALPS motifs. The ALPS1 motif may be sufficient for detection of a change in curvature of membranes with a high level of acyl chain unsaturation, whereas two functional ALPS motifs may be required for detection of a similar change for membranes with a low level of unsaturated lipids.

To test this hypothesis, we replaced a fraction (30%) of the most abundant lipids in our liposome formulation (egg PC and liver PE) with synthetic dioleoyl species (C18:1/C18:1/PC and C18:1/C18:1/PE) and used the GAP activity assay to evaluate the response of ArfGAP1 to membrane curvature. As expected, the incorporation of dioleyl lipids shifted the membrane curvature response toward larger liposome radii. As a result, the response to membrane curvature of the V279D mutant, in which only ALPS1 is

functional, resembles that of the wild-type form in the presence of classical Golgi-mix liposomes.

DISCUSSION

We have shown that mammalian ArfGAP1 contains a second motif, ALPS2, similar in terms of physical chemistry to the previously identified ALPS1 motif. Both motifs are intrinsically unstructured but fold in a synergic manner into amphipathic α-helices at the surface of curved membranes (Figure 2). They differ from classical membrane-adsorbing α-helices by the abundance of S/T residues in the polar face (Figure 1), a feature that explains their preference for membranes with packing defects such as those induced by membrane curvature (G. Drin, personal communication). Although the sharp response of ArfGAP1 to membrane curvature is primary due to the folding and/or adsorption of the ALPS1 motif, our results suggest that the combinatory use of two ALPS motifs tunes the range of curvature at which ArfGAP1 responds and/or adapts ArfGAP1 to membranes of various lipid compositions.

ALPS2 displays less avidity for highly curved lipid membranes than ALPS1 does (Figures 2 and 5). Although the physical chemistry of the two motifs seems similar (Figure 1), subtle differences may explain this observation. First, bulky hydrophobic residues (e.g., W, L, and I) are more abundant in the nonpolar face of ALPS1 than in the cognate face of ALPS2, which contains five Val residues (Figure 1C). Second, the ALPS1 motif may be longer than ALPS2. In the helical-wheel representations shown in Figure 1C, we assume that ALPS1 spans residues 199−234. These limits were suggested by a sequence alignment with the yeast homologue Gcs1p (*16*). However, the C-terminus of ALPS1 may extend beyond residue 234. First, the sequence between residues 235 and 251 of ArfGAP1, although not as hydrophobic as the sequence of residues 199−234, keeps a reasonable amphipathic character and is rich in S/T residues (Figure 1B). Second, we noticed previously that the fragment of residues 192−257 displays more robust liposome binding than the fragment of residues 192−231 (*16*). Last, at a saturating concentration of small liposomes, the level of helical structure of the peptide of residues 192−304 estimated by CD measurements is ∼80%, corresponding to 90 amino acids (Figure 2C), which is more than the sum of the length of the ALPS1 and ALPS2 sequences suggested in Figure 1 (36 and 32 residues, respectively).

Whatever the exact C-terminus of ALPS1, it is likely that there is some structural discontinuity between ALPS1 and ALPS2. Indeed, a continuous straight α-helix consisting of ALPS1 and ALPS2 seems to be ruled out since it could not interact with a curved membrane all along its length. Kinks are required to accommodate the curvature of the membrane, and this could be the role of a Pro residue (P254) between the two motifs, which should interrupt or at least distort the helical conformation locally. In addition, the sequence around this proline is not "in phase" with the proposed ALPS α-helices, since a continuous α-helix would put negatively charged residues such as E257 and E261 in the nonpolar face. In the future, additional mutations and structural approaches such as NMR or site-directed spin labeling combined with electron paramagnetic resonance spectroscopy will be required to gain a precise picture of the membrane-

bound conformation of the entire ALPS1−ALPS2 region and to better define the boundaries of the ALPS motifs. Such approaches have been successfully applied to α-synuclein, a small presynaptic protein, whose misfolding is associated with Parkinson's disease. Interestingly, α-synuclein also binds preferentially to highly curved membranes through the adsorption and folding of its first 90 amino acids into a structure composed of two α-helices joined by a flexible tether (*27−30*).

Several lines of evidence suggest a synergy between the two ALPS motifs for their folding and adsorption onto highly curved liposomes. First, the ALPS1−ALPS2 peptide binds to small liposomes and adopts an α-helical conformation much more readily than the individual motifs (Figures 2C and 5). Second, whereas the introduction of a membrane repulsive charge in a single ALPS motif results in a modest decrease in the activity of full-length ArfGAP1, the combination of two mutations, one in each motif, leads to a more severe inhibition (Figure 4B). As explained above, it is unlikely that the two ALPS motifs form a single continuous helix, and therefore, it is hard to imagine how the folding of one motif could propagate up to the second motif. Thus, the apparent synergy between the two ALPS motifs for their folding and adsorption onto curved membranes probably results from a reduction of dimensionality, an effect that applies to many membrane-binding modules (*22*). When one ALPS motif binds, the neighboring ALPS motif is confined in the vicinity of the membrane and therefore experiences a much higher lipid concentration as compared to an isolated ALPS motif. Therefore, even if the intrinsic avidity of ALPS2 for a curved lipid membrane is low, this is sufficient to drive strong binding, provided that ALPS1 is already bound.

What could be the advantage of having two ALPS motifs versus one? This issue is not obvious considering the fact that ArfGAP1 remains highly sensitive to membrane curvature when the ALPS2 motif is entirely deleted, such as in the construct of residues 1−257 (*16*) or when it is made nonfunctional by the highly perturbing V279D mutation (Figures 6B and 7). Moreover, several proteins of the ArfGAP1 subfamily lack the ALPS2 motif. The yeast homologue of ArfGAP1, Gcs1p, contains a region homologous to ALPS1 but not to ALPS2 (*16*). In mammals, an abundant isoform of ArfGAP1 has been found in the brain, which differs from the original ArfGAP1 protein by a large deletion in the ALPS2 motif (Δ259−280) and by an insertion of 10 residues downstream from the ALPS1 motif (*18*). One intriguing model, is suggested by the activity measurements shown in Figure 7: changing the number (or length) of the ALPS motifs could be a way for ArfGAP1 to adapt to the lipid composition of membranes. The response of ArfGAP1 to membrane curvature is very sharp as decreasing the diameter of Golgi-like liposomes from 80 to 40 nm results in a 20-fold increase in the activity of wild-type ArfGAP1 (Figure 6B). During the budding of a COPI-coated vesicle, such an almost all-or-none response should be advantageous, as Arf1 molecules would be lost by GTP hydrolysis only when membrane curvature has reached a given threshold. This threshold can be considered as the morphological limit between a young and shallow bud, for which coat stability would be compromised if too many Arf molecules were lost, and a mature bud, more curved and ready for fission, for which coat disassembly must be programmed. However, the
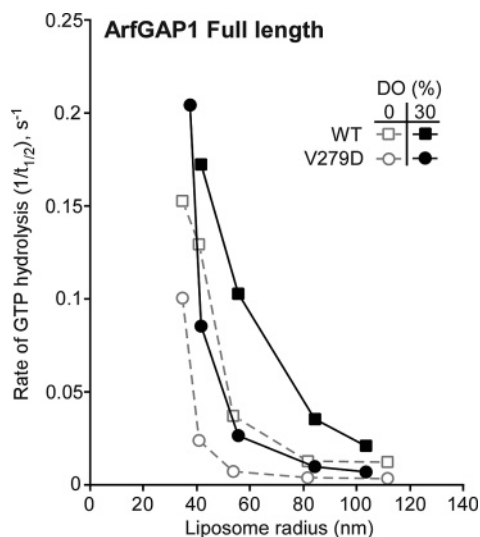
FIGURE 7: Changing the average acyl chain composition of the membrane shifts the response of ArfGAP1 to membrane curvature. GAP experiments similar to those shown in Figure 6B were performed with wild-type ArfGAP1 or with the V279D mutant on Golgi-mix liposomes in which a fraction (30 mol %) of egg PC and liver PE was replaced with dioleyl lipids. For comparison, the results from Figure 6 with the standard Golgi-mix composition are shown in gray.

very sharp response of ArfGAP1 to membrane curvature is also highly dependent on the lipid composition (Figure 7) (*11*, *16*, *19*). This is because defects in lipid packing depend on both the actual curvature of the bilayer and the lipid geometry (*31*). Therefore, to keep the response within a defined range of curvature (say between 80 and 40 nm), the adsorption energy of ArfGAP1 has to be adjusted according to the lipid composition of the membrane and notably to the ratio between conical and nonconical lipids. As this ratio differs not only between organisms but also between tissues (e.g., the brain contains more unsaturated lipids than the liver), the existence of tissue-specific ArfGAP1 isoforms that differ essentially by the length and number of functional ALPS motifs (*18*) could be a way to adapt to different lipid environments.

ACKNOWLEDGMENT

REFERENCES

1. Rothman, J. E., and Wieland, F. T. (1996) Protein sorting by transport vesicles, *Science 272*, 227−234.
2. Lee, M. C., Miller, E. A., Goldberg, J., Orci, L., and Schekman, R. (2004) Bi-directional protein transport between the ER and Golgi, *Annu. Rev. Cell Dev. Biol. 20*, 87−123.
3. McMahon, H. T., and Mills, I. G. (2004) COP and clathrin-coated vesicle budding: Different pathways, common approaches, *Curr. Opin. Cell Biol. 16*, 379−391.
4. Antonny, B. (2006) Membrane deformation by protein coats, *Curr. Opin. Cell Biol. 18*, 386−394.
5. Nie, Z., and Randazzo, P. A. (2006) Arf GAPs and membrane traffic, *J. Cell Sci. 119*, 1203−1211.
6. Goldberg, J. (1999) Structural and functional analysis of the ARF1-ARFGAP complex reveals a role for coatomer in GTP hydrolysis, *Cell 96*, 893−902.
7. Eugster, A., Frigerio, G., Dale, M., and Duden, R. (2000) COP I domains required for coatomer integrity, and novel interactions with ARF and ARF-GAP, *EMBO J. 19*, 3905−3917.
8. Lee, S. Y., Yang, J. S., Hong, W., Premont, R. T., and Hsu, V. W. (2005) ARFGAP1 plays a central role in coupling COPI cargo sorting with vesicle formation, *J. Cell Biol. 168*, 281−290.
9. Aoe, T., Huber, I., Vasudevan, C., Watkins, S. C., Romero, G., Cassel, D., and Hsu, V. W. (1999) The KDEL receptor regulates a GTPase-activating protein for ADP-ribosylation factor 1 by interacting with its non-catalytic domain, *J. Biol. Chem. 274*, 20545−20549.
10. Rein, U., Andag, U., Duden, R., Schmitt, H. D., and Spang, A. (2002) ARF-GAP-mediated interaction between the ER-Golgi v-SNAREs and the COPI coat, *J. Cell Biol. 157*, 395−404.
11. Antonny, B., Huber, I., Paris, S., Chabre, M., and Cassel, D. (1997) Activation of ADP-ribosylation factor 1 GTPase-activating protein by phosphatidylcholine-derived diacylglycerols, *J. Biol. Chem. 272*, 30848−30851.
12. Wong, T. A., Fairn, G. D., Poon, P. P., Shmulevitz, M., McMaster, C. R., Singer, R. A., and Johnston, G. C. (2005) Membrane metabolism mediated by Sec14 family members influences Arf GTPase activating protein activity for transport from the trans-Golgi, *Proc. Natl. Acad. Sci. U.S.A. 102*, 12777−12782.
13. Yanagisawa, L. L., Marchena, J., Xie, Z., Li, X., Poon, P. P., Singer, R. A., Johnston, G. C., Randazzo, P. A., and Bankaitis, V. A. (2002) Activity of specific lipid-regulated ADP ribosylation factor-GTPase-activating proteins is required for Sec14p-dependent Golgi secretory function in yeast, *Mol. Biol. Cell 13*, 2193−2206.
14. Cukierman, E., Huber, I., Rotman, M., and Cassel, D. (1995) The ARF1 GTPase-activating protein: Zinc finger motif and Golgi complex localization, *Science 270*, 1999−2002.
15. Liu, W., Duden, R., Phair, R. D., and Lippincott-Schwartz, J. (2005) ArfGAP1 dynamics and its role in COPI coat assembly on Golgi membranes of living cells, *J. Cell Biol. 168*, 1053−1063.
16. Bigay, J., Casella, J. F., Drin, G., Mesmin, B., and Antonny, B. (2005) ArfGAP1 responds to membrane curvature through the folding of a lipid packing sensor motif, *EMBO J. 24*, 2244−2253.
17. Yu, S., and Roth, M. G. (2002) Casein kinase I regulates membrane binding by ARF GAP1, *Mol. Biol. Cell 13*, 2559−2570.
18. Parnis, A., Rawet, M., Regev, L., Barkan, B., Rotman, M., Gaitner, M., and Cassel, D. (2006) Golgi Localization Determinants in ArfGAP1 and in New Tissue-specific ArfGAP1 Isoforms, *J. Biol. Chem. 281*, 3785−3792.
19. Bigay, J., Gounon, P., Robineau, S., and Antonny, B. (2003) Lipid packing sensed by ArfGAP1 couples COPI coat disassembly to membrane bilayer curvature, *Nature 426*, 563−566.
20. Bigay, J., and Antonny, B. (2005) Real-time assays for the assembly-disassembly cycle of COP coats on liposomes of defined size, *Methods Enzymol. 404*, 95−107.
21. Ladokhin, A. S., Jayasinghe, S., and White, S. H. (2000) How to measure and analyze tryptophan fluorescence in membranes properly, and why bother? *Anal. Biochem. 285*, 235−245.
22. Buser, C. A., Sigal, C. T., Resh, M. D., and McLaughlin, S. (1994) Membrane binding of myristylated peptides corresponding to the NH2 terminus of Src, *Biochemistry 33*, 13093−130101.
23. Antonny, B., Beraud-Dufour, S., Chardin, P., and Chabre, M. (1997) N-Terminal hydrophobic residues of the G-protein ADP-ribosylation factor-1 insert into membrane phospholipids upon GDP to GTP exchange, *Biochemistry 36*, 4675−4684.
24. Sreerama, N., and Woody, R. W. (2000) Estimation of protein secondary structure from circular dichroism spectra: Comparison of CONTIN, SELCON, and CDSSTR methods with an expanded reference set, *Anal. Biochem. 287*, 252−260.
25. Gaboriaud, C., Bissery, V., Benchetrit, T., and Mornon, J. P. (1987) Hydrophobic cluster analysis: An efficient new way to compare and analyse amino acid sequences, *FEBS Lett. 224*, 149−155.
26. Che, M. M., Boja, E. S., Yoon, H. Y., Gruschus, J., Jaffe, H., Stauffer, S., Schuck, P., Fales, H. M., and Randazzo, P. A. (2005) Regulation of ASAP1 by phospholipids is dependent on the interface between the PH and Arf GAP domains, *Cell. Signalling 17*, 1276−1288.
27. Davidson, W. S., Jonas, A., Clayton, D. F., and George, J. M. (1998) Stabilization of α-synuclein secondary structure upon binding to synthetic membranes, *J. Biol. Chem. 273*, 9443−9449.
28. Chandra, S., Chen, X., Rizo, J., Jahn, R., and Sudhof, T. C. (2003) A broken α-helix in folded α-Synuclein, *J. Biol. Chem. 278*, 15313−15318.

29. Bisaglia, M., Tessari, I., Pinato, L., Bellanda, M., Giraudo, S., Fasano, M., Bergantino, E., Bubacco, L., and Mammi, S. (2005) A topological model of the interaction between α-synuclein and sodium dodecyl sulfate micelles, *Biochemistry 44*, 329−339.

30. Ulmer, T. S., Bax, A., Cole, N. B., and Nussbaum, R. L. (2005) Structure and dynamics of micelle-bound human α-synuclein, *J. Biol. Chem. 280*, 9595−9603.

31. van den Brink-van der Laan, E., Killian, J. A., and de Kruijff, B. (2004) Nonbilayer lipids affect peripheral and integral membrane proteins via changes in the lateral pressure profile, *Biochim. Biophys. Acta 1666*, 275−288.